Solubilities of CO and H_2 in Neat and CO_2-Expanded Hydroformylation Reaction Mixtures Containing 1-Octene and Nonanal up to 353.15 K and 9 MPa†

Zhuanzhuan Xie, William K. Snavely, Aaron M. Scurto, and Bala Subramaniam*

Center for Environmentally Beneficial Catalysis, Department of Chemical & Petroleum Engineering, University of Kansas, Lawrence, Kansas 66045-7609

Accurate knowledge of the phase equilibria of CO_2-expanded hydroformylation reaction mixtures is essential to rational process design and development. Vapor−liquid equilibria of the following systems were measured in a variable-volume view cell at temperatures ranging from (313.15 to 353.15) K and pressures up to 9 MPa: CO + 1-octene, CO_2 + 1-octene, CO + 1-octene + CO_2, CO + nonanal, CO_2 + nonanal, CO + nonanal + CO_2, H_2 + 1-octene, H_2 + 1-octene + CO_2, H_2 + nonanal, and H_2 + nonanal + CO_2. The measured solubilities of CO and H_2 in the liquid phases were consistent with literature values. The presence of CO_2 was found to enhance the solubilities of both CO and H_2 in the liquid phase. The enhancement factor is up to 1.54 for carbon monoxide and 1.82 for hydrogen. The Peng−Robinson equation of state (PR EoS) with van der Waals mixing rules and binary interaction parameters modeled the VLE data adequately, with much better fits for the 1-octene systems compared to the more polar nonanal systems.

Introduction

The use of a new class of solvents, CO_2-expanded liquids (CXLs), as reaction media has received increased attention in recent years.[1] A CXL is a mixture composed of subcritical CO_2 condensed into an organic solvent. By varying the CO_2 composition, a continuum of liquid media ranging from the neat organic solvent to compressed CO_2 is generated, the properties of which can be adjusted by tuning the operating pressure. For 1-olefin hydroformylation, CXLs have been shown to increase turnover frequencies while also enhancing selectivity toward the desired linear aldehyde.[2] Accurate knowledge of the phase equilibria of CO_2-expanded hydroformylation reaction mixtures is essential to rational process design and development.

A large number of publications may be found on the vapor−liquid equilibrium of CO (or H_2) + organic liquid and CO (or H_2) + CO_2 binary systems. Table 1 lists some systems of interest. In the range of temperatures and pressures reported in these referenced studies, the CO and H_2 solubilities in the liquid phase follow Henry's law.

In contrast, relatively few publications were found dealing with CO (and/or H_2) + CO_2 + organic liquid ternary and quaternary systems. The emerging interest in CXLs as solvent media for catalytic reactions, especially those involving gaseous reactants (such as in hydrogenation, oxidation, carbonylation, and hydroformylation), has led to increased research into the phase equilibria of (gas + CO_2 + organic/inorganic liquid) type systems. Table 2 lists some systems of interest. To date, the solubility studies in CO_2-expanded liquids are still very limited and system-specific in nature.

Modeling of CXL systems has also been performed. Houndonougbo et al.[17,18] used Monte Carto and molecular dynamics to simulate the phase equilibria and transport properties in carbon dioxide expanded acetonitrile, methanol, ethanol, acetone, acetic acid, toluene, and 1-octene. Guha et al.[19] showed a detailed reactor model incorporating reaction kinetics, mass transfer rates, and phase equilibrium to systematically investigate the effects of mass transfer and catalyst activation on the induction period in 1-octene hydroformylation in CXL. Such experimental measurements, combined with complementary modeling studies using empirical equation of states or molecular simulation methods, are essential to gain a better fundamental understanding of the continuum of CXL media and to their rational application in many multiphase catalytic processes. Accordingly, this paper reports measurements of the intrinsic solubilities of CO and H_2 in CO_2-expanded hydroformylation mixtures including the reactant (1-octene) and product (nonanal) under pressures and temperatures encountered in homogeneous catalytic hydroformylation (up to 353.15 K and 9 MPa). Predictive thermodynamic models are also developed to describe vapor−liquid equilibria of the investigated binary and ternary systems.

Experimental

The apparatus (Figure 1) for measuring solubility of hydrogen and carbon monoxide in CO_2-expanded 1-octene or nonanal mixtures consists of a SFT phase monitor II (Supercritical Fluid Technologies, Inc.), two Valco four-port valves (Valco Instruments Co., Inc.), a Micropump (IDEX corporation), a syringe pump (model 500D, Teledyne Isco, Inc.), the liquid and gas sampling valves (Valco Instruments Co., Inc.) in the gas chromatograph (GC, Varian CP-3800), and a Camile 3300 data acquisition and control system.

The SFT phase monitor II consists of a manually controlled syringe pump integrated within a 30 mL view cell. The volume of the view cell can be varied from (3 to 30) mL. A CCD camera with a fiber optic light source allows clear viewing of the cell's interior. The image is displayed on the TV/VCR monitor. The view cell can be oriented in a horizontal position for solubility work with liquid materials and in a vertical configuration for solubility work with solid materials. The sample holder accommodates liquid, solid, and powder samples. Fluid mixing is achieved through rare earth magnets coupled to an internally

* Corresponding author. Tel.: +1 785-864-2903. Fax: +1 785-864-6051. E-mail: bsubramaniam@ku.edu.
† Part of the "Gerhard M. Schneider Festschrift".

10.1021/je900148e CCC: $40.75
Published on Web 04/09/2009

Table 1. Reported Solubility Measurements of Binary Systems Involving CO, H_2, or CO_2 (1) and Organic Liquids (2) at Temperature *T* and Pressure *p*

(1)	(2)	*T*/K	*p*/MPa	ref
CO_2	acetone, methanol	298.15, 313.15	0.4 to 7.3	3
H_2	10 organic solvents	298.15, 323.15, 373.15	≤ 10	4
H_2, CO	1-octene, acetone, acetonitrile, water, ethanol	298.15, 323.15	0.3 to 2.0	5
H_2, CO	water, octane, toluene, nonanal	353, 363, 373	0.5 to 1.5	6
CO	CO_2 (liquid)	283	0.6 to 14	7, 8
gases (including CO_2, H_2, CO)	organic liquids			9 (review)
CO_2	alkanes		high pressure	10 (review)

Table 2. Reported Solubility Measurements of Ternary Systems Involving CO or H_2 (1) in CO_2-Expanded Organic Liquids (2) at Temperature *T* and Pressure *p*

(1)	(2)	*T*/K	*p*/MPa	ref
H_2	methanol	278, 288, 298	≤ 20	11
H_2	methanol	313	21.7	12
H_2	toluene	305 to 343	1.2 to 10.5	13
O_2, CO	acetonitrile, acetone, methanol	298 to 313	≤ 9	14
H_2	2-propanol	298, 333	H_2 partial pressure ≤ 6	15
H_2	acetonitrile, acetone, methanol	313	2.5, 6, 9	16

mounted impeller as well as the circulation of the fluid. An internal resistance temperature detector (RTD) is used to measure the temperature. A fuzzy logic controller (AI-100, Total Temperature Instrumentation, Inc.) uniformly controls the heating of the view cell up to 423 K with an uncertainty of ± 0.5 K. The pressure gauge is composed of a pressure transducer and an Analog Input Panel Meter (Red Lion Controls, Inc.) with an uncertainty of ± 13.8 kPa in pressures ranging from vacuum to 20 MPa.

In a typical run, the cell is evacuated down to a subambient pressure and preflushed with CO_2 several times to remove any residual air. A predetermined amount of the liquid mixture is syringed into the cell, followed by addition of a pure gas (CO or H_2) or gas mixtures (H_2 + CO_2 or CO + CO_2 with certified compositions by gas suppliers) from the top of the view cell. The system is then brought to the set temperature, stirred, and allowed to equilibrate for at least one hour. A micropump is employed to circulate the liquid through the vapor phase to mix and achieve equilibrium. At each equilibrated pressure, samples are withdrawn from both the vapor and liquid phases and analyzed using an online GC. Three repeated samples were taken for each equilibrated pressure. The vapor phase is sampled by the static gas sampling method by withdrawing a small amount of gas from the top of the view cell. A capillary tubing with 0.015″ ID × 1/16″ OD × 56″ L is used as a sample transfer line. The pressure drop in the cell upon sampling is usually less than 1 bar. Following each sampling, the pressure is maintained constant by suitably moving the piston. The atmospheric balancing[20] technique was used here to load the sample loop with the gas sample. Atmospheric balancing involved shutting off the sample flow and allowing the pressure in the sample loop to equilibrate with atmospheric pressure at a constant temperature, prior to injection. In this manner, an identical molar amount of the various samples was injected into the GC column. The liquid samples were injected directly under pressure from the LSV.

During each sample withdrawal, two sample loops in each sampling valve are filled simultaneously to enable parallel analysis, where the nonpolar gas components are analyzed by the thermal conductivity detector (TCD) and the organic components by a flame ionization detector (FID). The liquid sampling valve is 8-port with two sampling loops measuring (0.2 and 0.5) μL in internal volume. The 0.2 μL sample is injected to the TCD. The gas sampling valve is 10-port with (200 and 250) μL external sample loops. The 200 μL sample is injected to the TCD. The capillary column used for measuring the liquid phase composition was a Varian CP-Wax 52CB, 50 m × 0.25 mm × 0.2 μm, with helium carrier gas. The packed columns used for measuring gas phase composition were a precolumn (4′ × 1/16″, 1.5 % OV-101 on Chromasorb GHP) from Supelco and a Hayesep D (6′ × 1/8″ SS, 80/100 mesh) from Hayes Separation, Inc.

1-Octene (99+ % purity) was obtained from Acros Organics; nonanal (lot purity ≥ 99 %) was obtained from Sigma-Aldrich,

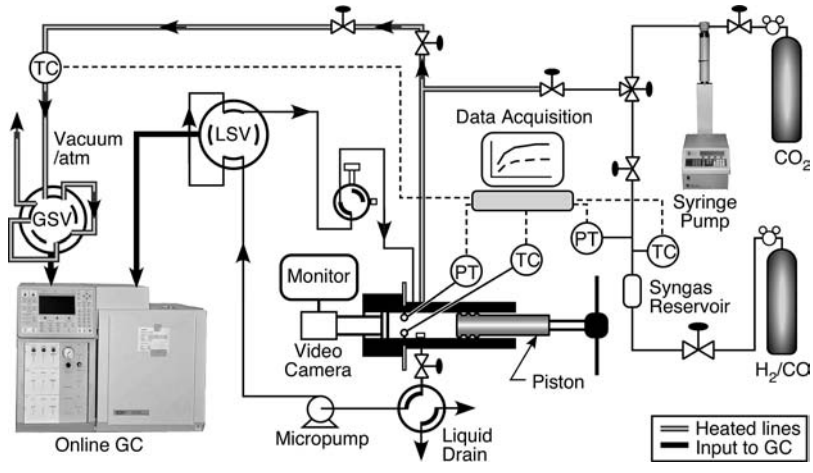

Figure 1. Apparatus for solubility measurements.

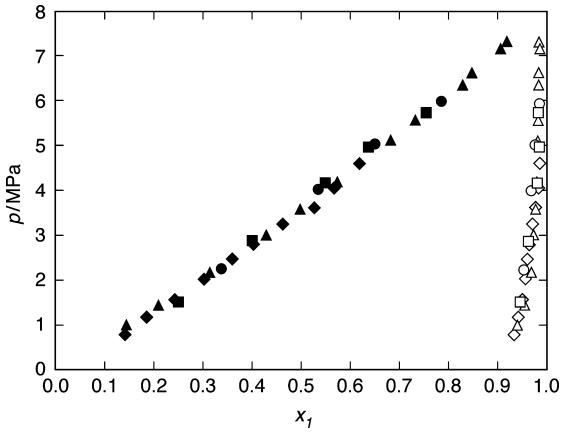

Figure 2. Vapor−liquid equilibrium of binary mixtures CO_2 (1) + acetone (2) at $T = 313.15$ K and pressure $p =$ (0 to 8) MPa. Mole fractions x_1. ●, This work, run 1, liquid phase; ○, this work, run 1, vapor phase; ■, this work, run 2, liquid phase; □, this work, run 2, vapor phase; ◆, ref 21, liquid phase; ◇, ref 21, vapor phase; ▲, ref 3, liquid phase; and Δ, ref 3, vapor phase.

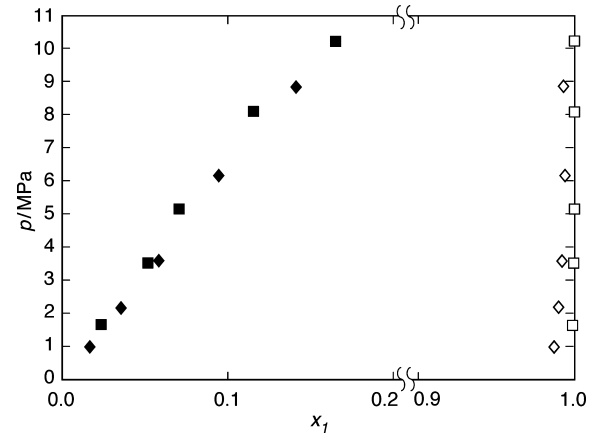

Figure 3. Vapor−liquid equilibrium of binary mixtures CO (1) + 1-octene (2) at $T = 333.15$ K and pressure $p =$ (0 to 11) MPa. Mole fractions x_1. ◆, This work, liquid phase; ◇, this work, vapor phase; ■, ref 22, liquid phase; and □, ref 22, vapor phase.

Inc.; and acetone (HPLC grade 99.9+ %) was acquired from Sigma-Aldrich, Inc. All organic compounds were used as received. Carbon dioxide (industrial grade, > 99.5 %), carbon monoxide (research grade, 99 %), hydrogen (ultrahigh purity, 99.99 %), and custom gas mixtures were purchased from Airgas, Inc. The CO_2 + CO gas mixture was 50.00 % CO_2 (molar), and the balance was CO; the CO_2 + H_2 gas mixture was 50.86 % CO_2 (molar), and the balance H_2.

Results and Discussion

To establish the reliability of the experimental unit and procedures, a set of benchmarking experiments aimed at reproducing published phase behavior data were performed. The vapor−liquid equilibrium (VLE) of the CO_2 + acetone binary system was measured at 313.15 K and pressures between (1 and 9) MPa. The VLE data are plotted in Figure 2. The measurement errors are within the size of the data points in this and subsequent figures. The phase equilibrium data of CO_2 in neat acetone reported by Day[21] and Katayama[3] at 313.15 K are also included in Figure 2. The experimental data obtained in this work match well with Day and Katayama's data.

The vapor−liquid equilibria of the CO and 1-octene mixture at 333.15 K and pressures between (1 and 9) MPa were measured and compared with the data of Jin[22] (Figure 3). The data from this work match well with Jin's data.

The phase equilibrium of the ternary system CO_2 + CO + acetone at 313.15 K and 9 MPa was investigated with different gas compositions. As seen from Figure 4, the experimental data from this work display a trend identical to the literature data (Lopez Castillo et al.[14]), and the ends of the tie lines from the two sets of data appear to form a smooth two-phase envelope.

The accumulated uncertainty for measuring gas and liquid compositions by the GC method is calculated following Bonate's[23−26] methods. The uncertainty is less than 5 % for the cases studied.

CO_2 + CO + 1-Octene. The vapor−liquid equilibrium of CO and 1-octene mixtures was measured at (313.15, 333.15, and 353.15) K and at pressures between (1 and 9) MPa at each temperature. The data are shown in Table 3 and plotted in Figure 5. In general, the solubility of CO increases with an increase in total pressure. In contrast, temperature has a weak effect on CO solubility in the liquid phase.

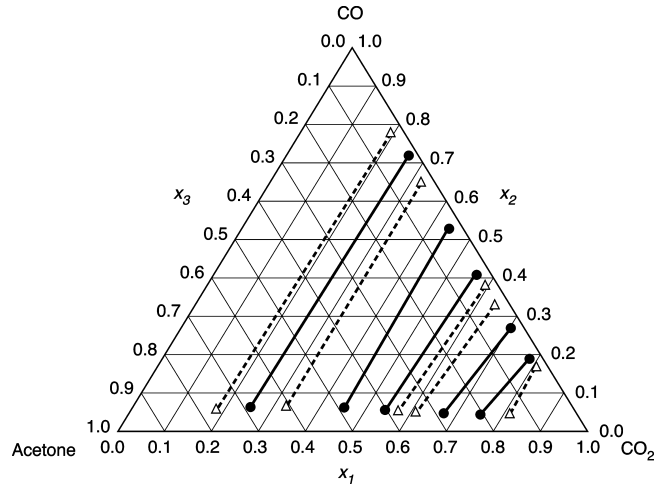

Figure 4. Vapor−liquid equilibrium of ternary mixtures CO_2 (1) + CO (2) + acetone (3) at $T = 313.15$ K and $p = 9$ MPa. Mole fractions x_i. --Δ--, This work; and —●—, ref 14.

Table 3. Vapor Phase Mole Fraction y_1, Standard Deviation δy_1, Liquid Phase Mole Fraction x_1, and Standard Deviation δx_1 for CO (1) + 1-Octene (2) Binary Mixtures at $T =$ (313.15, 333.15, and 353.15) K and Total p from (0 to 9) MPa

T/K	p/MPa	x_1	δx_1	y_1	δy_1
313.15	0.93	0.015	0.001	0.992	0.001
313.15	2.20	0.036	0.001	0.995	0.001
313.15	4.10	0.068	0.001	0.996	0.001
313.15	5.40	0.087	0.003	0.997	0.001
313.15	7.23	0.116	0.005	0.997	0.001
313.15	8.55	0.141	0.002	0.996	0.001
333.15	1.00	0.017	0.001	0.987	0.001
333.15	2.20	0.036	0.001	0.990	0.001
333.15	3.60	0.058	0.001	0.992	0.001
333.15	6.17	0.095	0.001	0.994	0.001
333.15	8.88	0.141	0.006	0.993	0.001
353.15	1.34	0.021	0.001	0.967	0.003
353.15	2.20	0.036	0.002	0.982	0.000
353.15	4.62	0.074	0.003	0.988	0.001
353.15	6.16	0.095	0.001	0.989	0.001
353.15	8.45	0.127	0.004	0.983	0.009

The vapor−liquid equilibrium data for CO_2 and 1-octene binary mixtures at (313.15, 333.15, and 353.15) K at pressures between (1 and 9) MPa are shown in Table 4 and plotted in Figure 6. The standard deviations are within the size ranges of the data points. As expected, the CO_2 solubility in 1-octene

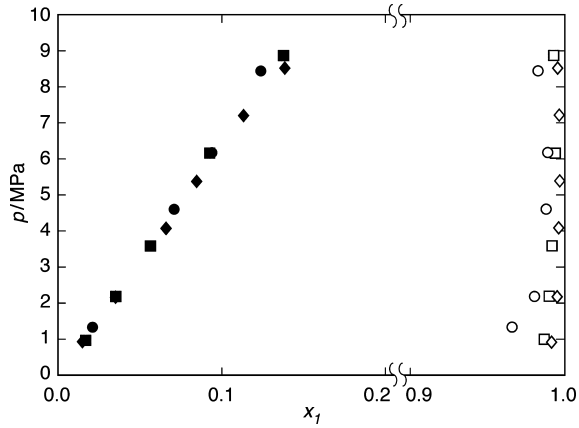

Figure 5. Vapor−liquid equilibrium of binary mixtures CO (1) + 1-octene (2) at pressure p = (0 to 9) MPa. Mole fractions x_1. ◆, 313.15 K, liquid phase; ◇, 313.15 K, vapor phase; ■, 333.15 K, liquid phase; □, 333.15 K, vapor phase; ●, 353.15 K, liquid phase; and ○, 353.15 K, vapor phase.

Table 4. Vapor Phase Mole Fraction y_1, Standard Deviation δy_1, Liquid Phase Mole Fraction x_1, and Standard Deviation δx_1 for CO_2 (1) + 1-Octene (2) Binary Mixtures at T = (313.15, 333.15, and 353.15) K and Total p from (0 to 8) MPa

T/K	p/MPa	x_1	δx_1	y_1	δy_1
313.15	1.35	0.147	0.006	0.993	0.001
313.15	3.48	0.408	0.008	0.995	0.001
313.15	4.65	0.544	0.002	0.996	0.001
313.15	6.06	0.717	0.005	0.994	0.001
313.15	7.01	0.858	0.003	0.995	0.002
333.15	1.28	0.134	0.005	0.985	0.001
333.15	3.37	0.307	0.007	0.991	0.001
333.15	4.94	0.446	0.004	0.991	0.001
333.15	6.31	0.576	0.006	0.990	0.002
333.15	8.09	0.694	0.002	0.994	0.002
353.15	1.17	0.107	0.005	0.985	0.001
353.15	2.55	0.201	0.007	0.980	0.002
353.15	4.13	0.320	0.004	0.980	0.001
353.15	6.17	0.452	0.006	0.980	0.001
353.15	7.91	0.551	0.002	0.994	0.002

increases with an isothermal increase in pressure, while an increase in temperature reduces the CO_2 solubility in 1-octene.

The VLE phase equilibrium data of the CO_2 + CO + 1-octene ternary system at (313.15, 333.15, and 353.15) K at 8 MPa are provided in Table 5. The data in each row of the tables represent a tie line in a ternary diagram. Several different tie lines were obtained at a given pressure. The mole fractions of CO, CO_2, and 1-octene in each phase add up to unity. For clarity, only the CO_2 and CO mole fractions are shown in the table, with the balance being 1-octene. The standard deviations associated with the measurements and the VLE data simulated using HYSYS are also included in Table 5. Subsequent tables of ternary data follow a pattern similar to Table 5.

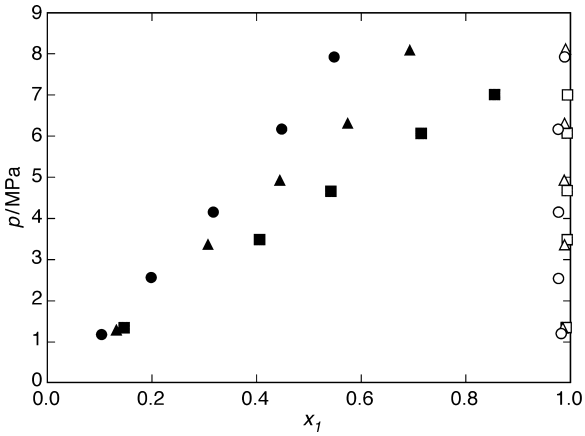

Figure 6. Vapor−liquid equilibrium of binary mixtures CO_2 (1) + 1-octene (2) at pressure p = (0 to 9) MPa. Mole fractions x_1. ■, 313.15 K, liquid phase; □, 313.15 K, vapor phase; ▲, 333.15 K, liquid phase; Δ, 333.15 K, vapor phase; ●, 353.15 K, liquid phase; and ○, 353.15 K, vapor phase.

Table 5. Vapor Phase Mole Fractions y_1, y_2, Standard Deviations δy_1, δy_2, Liquid Phase Mole Fractions x_1, x_2, and Standard Deviations δx_1, δx_2 for CO_2 (1) + CO (2) + 1-Octene (3) Ternary Mixtures at T = (313.15, 333.15, and 353.15) K and Total p = 8 MPa

vapor phase	T/K	y_1	δy_1	y_2	δy_2	y_1 (HYSYS)	y_2 (HYSYS)
	313.15	0.723	0.001	0.273	0.001	0.724	0.273
	313.15	0.614	0.003	0.382	0.003	0.614	0.382
	313.15	0.505	0.004	0.491	0.004	0.505	0.492
	313.15	0.440	0.006	0.556	0.006	0.440	0.556
liquid phase	T/K	x_1	δx_1	x_2	δx_2	x_1 (HYSYS)	x_2 (HYSYS)
	313.15	0.571	0.002	0.042	0.001	0.568	0.045
	313.15	0.485	0.000	0.056	0.002	0.472	0.058
	313.15	0.399	0.002	0.068	0.001	0.384	0.070
	313.15	0.347	0.002	0.074	0.001	0.334	0.077
vapor phase	T/K	y_1	δy_1	y_2	δy_2	y_1 (HYSYS)	y_2 (HYSYS)
	333.15	0.732	0.001	0.261	0.001	0.733	0.261
	333.15	0.645	0.003	0.348	0.003	0.646	0.348
	333.15	0.524	0.004	0.469	0.004	0.525	0.469
	333.15	0.420	0.006	0.573	0.006	0.421	0.573
liquid phase	T/K	x_1	δx_1	x_2	δx_2	x_1 (HYSYS)	x_2 (HYSYS)
	333.15	0.458	0.002	0.036	0.001	0.447	0.037
	333.15	0.403	0.000	0.047	0.002	0.392	0.049
	333.15	0.328	0.002	0.062	0.001	0.315	0.065
	333.15	0.262	0.002	0.074	0.001	0.251	0.077
vapor phase	T/K	y_1	δy_1	y_2	δy_2	y_1 (HYSYS)	y_2 (HYSYS)
	353.15	0.721	0.001	0.267	0.0009	0.719	0.267
	353.15	0.628	0.001	0.360	0.0004	0.627	0.360
	353.15	0.537	0.001	0.451	0.0002	0.536	0.451
	353.15	0.434	0.004	0.554	0.0035	0.435	0.554
liquid phase	T/K	x_1	δx_1	x_2	δx_2	x_1 (HYSYS)	x_2 (HYSYS)
	353.15	0.396	0.003	0.038	0.001	0.388	0.041
	353.15	0.345	0.002	0.050	0.001	0.335	0.053
	353.15	0.295	0.002	0.060	0.001	0.286	0.064
	353.15	0.239	0.003	0.073	0.001	0.232	0.076

Table 6. Critical Temperature T_c, Critical Pressure p_c, and Acentricity ω of the Substances

substance	T_c/K	p_c/MPa	ω
CO	134.45	3.499	0.093
CO_2	304.1	7.370	0.239
H_2	33.18	1.316	−0.120
acetone	508.0	4.700	0.304
1-octene	566.55	2.624	0.386
nonanal	658.5	2.330	0.592

The VLE data for the ternary systems were simulated at the experimental conditions by using the Peng−Robinson equation of state (PR EoS) with van der Waals mixing rules and binary interaction parameters. The critical parameters were obtained from the HYSYS library and are shown in Table 6. The binary interaction parameters were obtained from the literature. For systems lacking such information in the literature, the HYSYS simulator was used to generate the binary interaction parameters by fitting the experimental VLE data for the binary system. The

Table 7. Binary Interaction Parameters k_{ij} Used in the PR EoS at T = (313.15, 333.15, and 353.15) K

compounds	T/K	k_{ij}
CO_2 + CO	313.15	0.21[a]
	333.15	0.27[b]
	353.15	0.31[b]
CO_2 + H_2	313.15	0.31[a]
	333.15	0.40[b]
CO_2 + 1-octene	313.15	0.08[c]
	333.15	0.09[c]
	353.15	0.10[c]
CO + 1-octene	313.15	0.02[c]
	333.15	0.02[c]
	353.15	0.02[c]
H_2 + 1-octene	313.15	0.10[c]
	333.15	0.20[c]
CO_2 + nonanal	313.15	0.035[c]
	333.15	0.03[c]
CO + nonanal	313.15	0.07[c]
	333.15	0.09[c]
H_2 + nonanal	313.15	0.07[c]
	333.15	0.10[c]

[a] Used as reported. [b] Extrapolated from k_{ij} values fit to literature data. [c] From model fit of binary VLE data from this work.

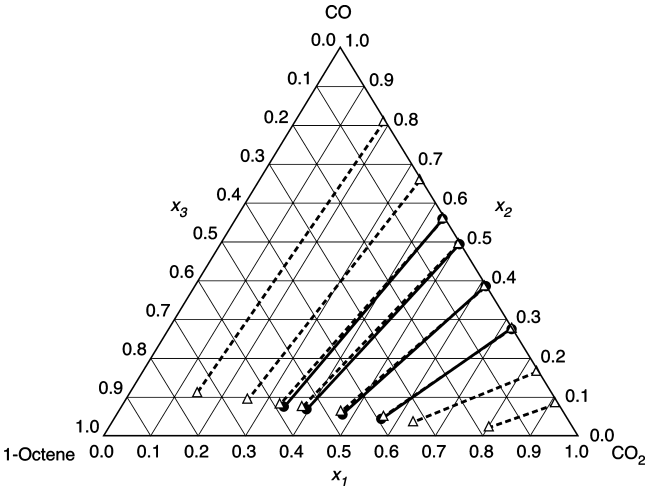

Figure 7. Vapor−liquid equilibrium of ternary mixtures CO_2 (1) + CO (2) + 1-octene (3) at T = 313.15 K and p = 8 MPa. Mole fractions x_i. —●—, Experimental data; and --Δ--, HYSYS simulation data.

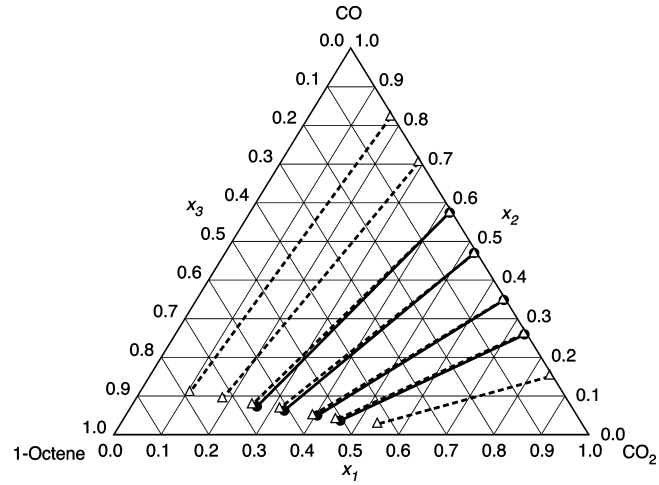

Figure 8. Vapor−liquid equilibrium of ternary mixtures CO_2 (1) + CO (2) + 1-octene (3) at T = 333.15 K and p = 8 MPa. Mole fractions x_i. —●—, Experimental data; and --Δ--, HYSYS simulation data.

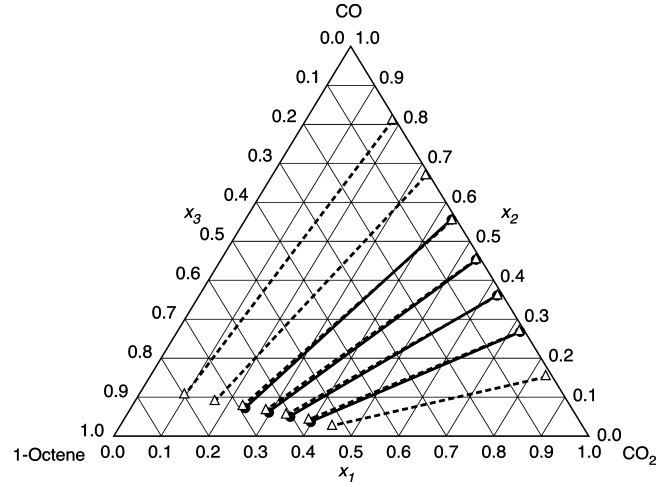

Figure 9. Vapor−liquid equilibrium of ternary mixtures CO_2 (1) + CO (2) + 1-octene (3) at T = 353.15 K and p = 8 MPa. Mole fractions x_i. —●—, Experimental data; and --Δ--, HYSYS simulation data.

objective function used for fitting is given by eq 1 with a convergence criterion of less than 10^{-4} for both liquid and vapor phase compositions. When data were not available at the temperatures of interest, k_{ij} values were either interpolated or extrapolated from the temperatures available. Table 7 summarizes the binary interaction parameters used in the simulation. The experimental vapor phase composition was used as the feed composition in the flash calculation. When no results were obtained in the two-phase region, then slightly richer organic compositions were used lying approximately in the same experimental tie line.

The experimental and simulated VLE data for the CO_2 + CO + 1-octene ternary system at (313.15, 333.15, and 353.15) K and 8 MPa are shown in Figures 7, 8, and 9, respectively. The experimental and calculated values were compared using the average absolute relative deviations (AARD) defined as follows

$$\mathrm{AARD} = \frac{1}{\mathrm{ND}} \sum_{1}^{\mathrm{ND}} \frac{|x_{\mathrm{exp}} - x_{\mathrm{cal}}|}{x_{\mathrm{exp}}} \qquad (1)$$

where ND stands for the number of data and x_{exp} and x_{cal} stand for the experimental and calculated mole fractions, respectively.

Since the experimental vapor phase compositions were used as feed composition, the modeling results of the vapor phase compositions fit extremely well with the experimental results. The results for the liquid phase compositions are reported in Table 8. For sake of brevity, the AARDs for the other systems studied are also included in this table. In general, the results matched the experimental data reasonably well. The good fit between the experimental data and simulated results is attributed to the fact that the CXL phase (compositions close to the 1-octene + CO_2 axis in Figures 7 to 9) is lean in CO and the gas phase (compositions closer to the CO + CO_2 axis) is lean in 1-octene, and these two phases may thus be approximated as pseudobinary systems.

To better understand the effect of CO_2 on the CO solubility, the CO solubilities in CO_2-expanded solvents are compared with the CO solubility in pure solvent (i.e., without CO_2) at the same temperature and identical CO fugacity in the gas phase. The CO fugacity coefficients at various total pressures were estimated using the Peng−Robinson equation of state. At the experimental conditions, the CO fugacity coefficients

Table 8. % AARD Values for Liquid Phase Mole Fractions (x_1, x_2, x_3) Based on Experimental Data and HYSYS Modeling Using the Peng−Robinson EoS for Various Systems

system		% AARD		
CO_2 (1) + CO (2) + 1-Octene (3)		x_1	x_2	x_3
T/K	313.15	2.68	3.03	1.31
	333.15	2.17	3.40	1.35
	353.15	2.20	5.08	0.69
CO_2 (1) + CO (2) + Nonanal (3)				
T/K	313.15	6.43	5.55	7.34
	333.15	9.24	8.88	8.87
CO_2 (1) + H_2 (2) + 1-Octene (3)				
T/K	313.15	5.78	3.98	6.60
	333.15	4.00	1.58	2.68
CO_2 (1) + H_2 (2) + Nonanal (3)				
T/K	313.15	7.39	8.48	8.00
	333.15	6.72	6.49	5.78

Table 9. Enhancement Factor EF of CO Solubility in Pure Octene (1) and CXL−Octene (2) as a Function of CO Fugacity f_{CO} at T = (313.15, 333.15, and 353.15) K

T/K	f_{CO}/MPa	x_1	x_2	EF
313.15	2.19	0.036	0.042	1.19
313.15	3.05	0.050	0.056	1.12
313.15	3.93	0.064	0.068	1.06
313.15	4.45	0.073	0.074	1.02
333.15	2.09	0.034	0.036	1.07
333.15	2.78	0.045	0.047	1.05
333.15	3.75	0.060	0.062	1.03
333.15	4.59	0.073	0.074	1.01
353.15	2.14	0.035	0.038	1.09
353.15	2.88	0.046	0.050	1.08
353.15	3.61	0.057	0.060	1.06
353.15	4.43	0.069	0.073	1.05

were found to be close to unity. An enhancement factor (EF) is defined as follows

$$\mathrm{EF} = \frac{x^{\mathrm{CXL}}}{x^{\text{neat solvent}}} \tag{2}$$

where x^{CXL} and $x^{\text{neat solvent}}$ represent the mole fractions of the permanent gas component in the CXL and neat solvent, respectively.

Table 10. Vapor Phase Mole Fraction y_1, Standard Deviation δy_1, Liquid Phase Mole Fraction x_1, and Standard Deviation δx_1 for CO (1) + Nonanal (2) Binary Mixtures at T = (313.15 and 333.15) K and Total p from (0 to 8) MPa

T/K	*p*/MPa	x_1	δx_1	y_1	δy_1
313.15	0.99	0.012	0.003	0.998	0.002
313.15	2.63	0.030	0.003	0.996	0.001
313.15	4.13	0.049	0.005	0.997	0.002
313.15	5.43	0.063	0.001	0.996	0.001
313.15	7.37	0.083	0.003	0.996	0.001
333.15	1.03	0.014	0.001	0.996	0.001
333.15	2.48	0.029	0.002	0.997	0.002
333.15	3.83	0.044	0.001	0.996	0.001
333.15	5.25	0.059	0.001	0.996	0.001
333.15	6.97	0.076	0.004	0.995	0.001

Table 11. Vapor Phase Mole Fraction y_1, Standard Deviation δy_1, Liquid Phase Mole Fraction x_1, and Standard Deviation δx_1 for CO_2 (1) + Nonanal (2) Binary Mixtures at T = (313.15 and 333.15) K and Total p from (0 to 9) MPa

T/K	*p*/MPa	x_1	δx_1	y_1	δy_1
313.15	0.95	0.163	0.006	0.995	0.002
313.15	2.62	0.354	0.003	0.997	0.003
313.15	4.21	0.535	0.003	0.996	0.002
313.15	6.22	0.735	0.003	0.994	0.001
313.15	7.98	0.920	0.002	0.995	0.002
333.15	1.20	0.161	0.001	0.995	0.001
333.15	1.95	0.226	0.002	0.994	0.002
333.15	3.25	0.337	0.007	0.994	0.001
333.15	5.00	0.475	0.002	0.996	0.003
333.15	6.77	0.598	0.007	0.995	0.001
333.15	8.54	0.743	0.006	0.995	0.002

Table 9 gives the EF values at (313.15, 333.15, and 353.15) K and the values used in its computation. In these tables, CO solubility in pure solvent is compared to CO solubility in CXL solvent at the same temperature and identical gas phase CO fugacity.

From Table 9, it may be seen that EF values greater than unity are obtained at all the conditions studied. At constant temperature and total pressure, the EF values increase with increasing CO_2 mole fraction in the liquid phase, as shown by a comparison with Table 5. This increase is attributed to the increase in free volume in the CO_2-expanded liquid phase that favors CO solubility.

CO_2 + CO + Nonanal. Figure 10 shows the vapor−liquid equilibrium data for the CO + nonanal system at (313.15 and 333.15) K and pressures between (1 and 8) MPa, which are summarized in Table 10. The standard deviations are within

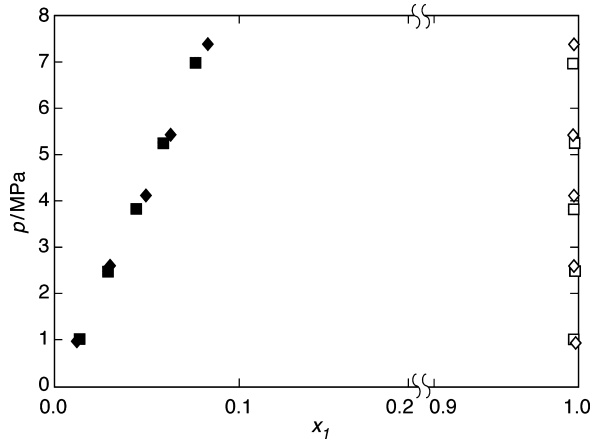

Figure 10. Vapor−liquid equilibrium of binary mixtures CO (1) + nonanal (2) at pressure p = (0 to 8) MPa. Mole fractions x_1. ◆, 313.15 K, liquid phase; ◇, 313.15 K, vapor phase; ■, 333.15 K, liquid phase; and □, 333.15 K, vapor phase.

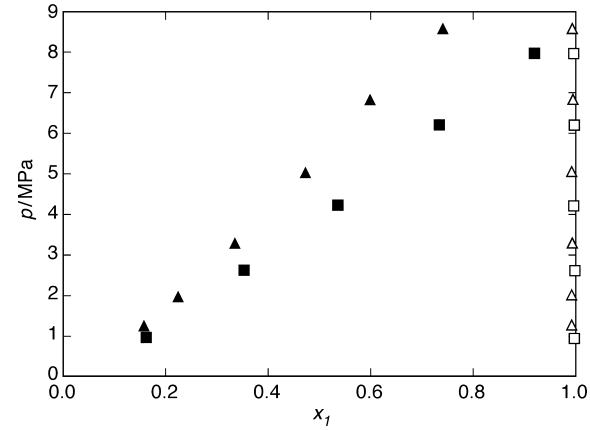

Figure 11. Vapor−liquid equilibrium of binary mixtures CO_2 (1) + nonanal (2) at pressure p = (0 to 9) MPa. Mole fractions x_1. ■, 313.15 K, liquid phase; □, 313.15 K, vapor phase; ▲, 333.15 K, liquid phase; and Δ, 333.15 K, vapor phase.

Table 12. Vapor Phase Mole Fraction y_1, y_2, Standard Deviation δy_1, δy_2, Liquid Phase Mole Fraction x_1, x_2, and Standard Deviation δx_1, δx_2 for CO_2 (1) + CO (2) + Nonanal (3) Ternary Mixtures at T = (313.15 and 333.15) K and Total p = 8 MPa

vapor phase	T/K	y_1	δy_1	y_2	δy_2	y_1 (HYSYS)	y_2 (HYSYS)
	313.15	0.464	0.001	0.529	0.002	0.465	0.535
	313.15	0.675	0.005	0.319	0.007	0.679	0.320
	313.15	0.791	0.003	0.206	0.003	0.792	0.208
	313.15	0.861	0.005	0.135	0.006	0.863	0.137
	313.15	0.589	0.002	0.396	0.002	0.596	0.404
liquid phase	T/K	x_1	δx_1	x_2	δx_2	x_1 (HYSYS)	x_2 (HYSYS)
	313.15	0.374	0.003	0.054	0.003	0.390	0.053
	313.15	0.613	0.002	0.037	0.002	0.559	0.036
	313.15	0.684	0.002	0.027	0.001	0.659	0.026
	313.15	0.762	0.004	0.021	0.002	0.728	0.019
	313.15	0.517	0.008	0.043	0.004	0.494	0.042
vapor phase	T/K	y_1	δy_1	y_2	δy_2	y_1 (HYSYS)	y_2 (HYSYS)
	333.15	0.379	0.013	0.615	0.009	0.380	0.620
	333.15	0.481	0.003	0.512	0.003	0.482	0.517
	333.15	0.610	0.003	0.384	0.003	0.612	0.388
	333.15	0.713	0.026	0.281	0.024	0.716	0.283
	333.15	0.830	0.003	0.162	0.003	0.834	0.165
liquid phase	T/K	x_1	δx_1	x_2	δx_2	x_1 (HYSYS)	x_2 (HYSYS)
	333.15	0.251	0.010	0.062	0.001	0.270	0.058
	333.15	0.379	0.005	0.053	0.002	0.337	0.050
	333.15	0.440	0.006	0.042	0.002	0.422	0.040
	333.15	0.536	0.009	0.033	0.001	0.490	0.031
	333.15	0.609	0.005	0.022	0.001	0.574	0.020

the size range of the plotted data points. As expected, the CO solubility increases with total pressure, while temperature has a relatively weak affect on the CO solubility. By comparison with Figure 5, CO is slightly less soluble in nonanal than in 1-octene.

The vapor−liquid equilibrium data for CO_2 and nonanal mixtures at (313.15 and 333.15) K at pressures between (1 and 8) MPa are shown in Table 11 and plotted in Figure 11. As expected, the CO_2 solubility in nonanal increases with total pressure and decreases at the higher temperature. By comparison with Figure 6, it is seen that CO_2 solubilities in nonanal and 1-octene are similar.

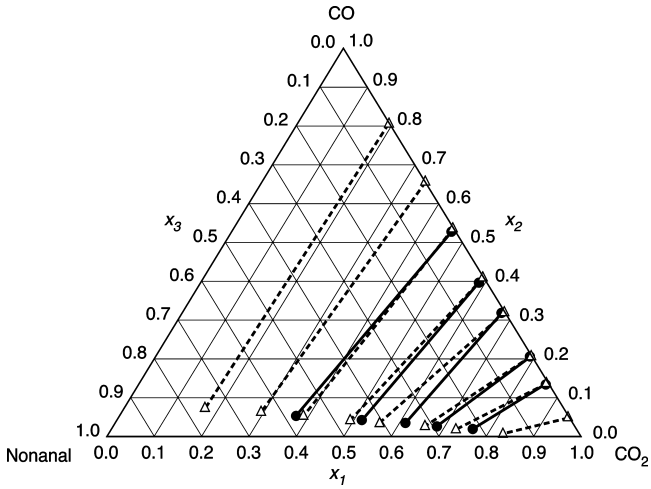

Figure 12. Vapor−liquid equilibrium of ternary mixtures CO_2 (1) + CO (2) + nonanal (3) at T = 313.15 K and p = 8 MPa. Mole fractions x_i. —●—, Experimental data; and --Δ--, HYSYS simulation data.

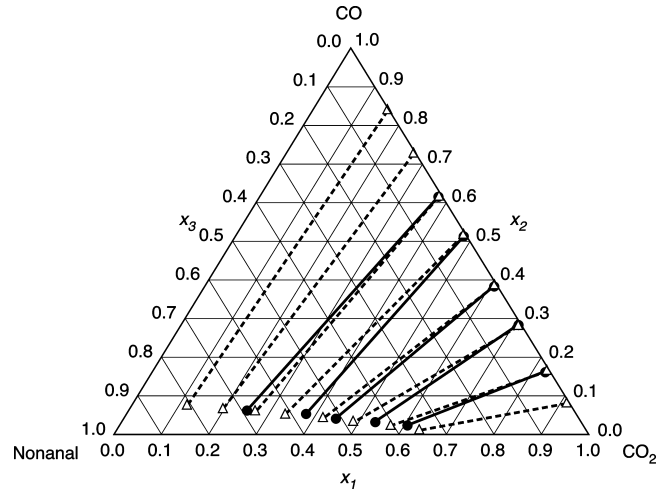

Figure 13. Vapor−liquid equilibrium of ternary mixtures CO_2 (1) + CO (2) + nonanal (3) at T = 333.15 K and p = 8 MPa. Mole fractions x_i. —●—, Experimental data; and --Δ--, HYSYS simulation data.

Table 13. Enhancement Factor EF of CO Solubility in Pure Nonanal (1) and CXL−Nonanal (2) as a Function of CO Fugacity f_{CO} at T = (313.15 and 333.15) K

T/K	f_{CO}/MPa	x_1	x_2	EF
313.15	1.06	0.014	0.021	1.54
313.15	1.61	0.020	0.027	1.35
313.15	2.49	0.030	0.037	1.22
313.15	3.10	0.037	0.043	1.18
313.15	4.14	0.049	0.054	1.11
333.15	1.28	0.017	0.022	1.35
333.15	2.22	0.027	0.033	1.24
333.15	3.04	0.035	0.042	1.19
333.15	4.05	0.046	0.053	1.15
333.15	4.87	0.055	0.062	1.12

The VLE data for CO_2 + CO + nonanal ternary mixtures at (313.15 and 333.15) K at 8 MPa are shown in Table 12, along with the simulated data. The experimental and simulated VLE data for this system are compared in Figures 12 and 13. Table 8 summarizes the fit between experimental and simulated VLE data using the average absolute relative deviations (AARD). In general, the experimental and simulated results show reasonably good agreement considering that only binary interaction parameters were used. The simulated results for nonanal-based systems are not as good as for 1-octene systems, presumably because the Peng−Robinson EoS works better for nonpolar or

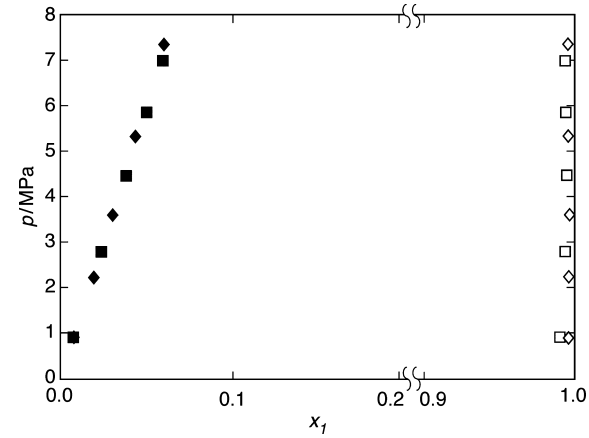

Figure 14. Vapor−liquid equilibrium of binary mixtures H_2 (1) + 1-octene (2) at pressure p = (0 to 8) MPa. Mole fractions x_1. ◆, 313.15 K, liquid phase; ◇, 313.15 K, vapor phase; ■, 333.15 K, liquid phase; and □, 333.15 K, vapor phase.

Table 14. Vapor Phase Mole Fraction y_1, Standard Deviation δy_1, Liquid Phase Mole Fraction x_1, and Standard Deviation δx_1 for H_2 (1) + 1-Octene (2) Binary Mixtures at T = (313.15 and 333.15) K and Total p from (0 to 8) MPa

T/K	p/MPa	x_1	δx_1	y_1	δy_1
313.15	0.93	0.008	0.001	0.995	0.001
313.15	2.27	0.019	0.001	0.995	0.001
313.15	3.63	0.031	0.001	0.996	0.001
313.15	5.35	0.043	0.003	0.995	0.001
313.15	7.36	0.060	0.006	0.995	0.001
333.15	0.94	0.008	0.000	0.989	0.001
333.15	2.81	0.024	0.001	0.993	0.001
333.15	4.48	0.038	0.001	0.994	0.002
333.15	5.86	0.050	0.002	0.993	0.001
333.15	7.00	0.059	0.001	0.993	0.001

Table 15. Vapor Phase Mole Fractions y_1, y_2, Standard Deviations δy_1, δy_2, Liquid Phase Mole Fractions x_1, x_2, and Standard Deviations δx_1, δx_2 for CO_2 (1) + H_2 (2) + 1-Octene (3) Ternary Mixtures at T = (313.15 and 333.15) K and Total p = 8 MPa

vapor phase	T/K	y_1	δy_1	y_2	δy_2	y_1 (HYSYS)	y_2 (HYSYS)
	313.15	0.231	0.002	0.762	0.006	0.237	0.762
	313.15	0.437	0.002	0.557	0.002	0.438	0.558
	313.15	0.621	0.004	0.374	0.003	0.622	0.375
	313.15	0.743	0.004	0.253	0.004	0.743	0.253
	313.15	0.838	0.004	0.157	0.004	0.838	0.157
liquid phase	T/K	x_1	δx_1	x_2	δx_2	x_1 (HYSYS)	x_2 (HYSYS)
	313.15	0.209	0.008	0.051	0.001	0.198	0.051
	313.15	0.373	0.010	0.040	0.002	0.350	0.041
	313.15	0.519	0.002	0.030	0.001	0.491	0.031
	313.15	0.607	0.009	0.023	0.001	0.596	0.024
	313.15	0.728	0.010	0.017	0.002	0.695	0.018
vapor phase	T/K	y_1	δy_1	y_2	δy_2	y_1 (HYSYS)	y_2 (HYSYS)
	333.15	0.531	0.005	0.463	0.004	0.531	0.464
	333.15	0.629	0.002	0.365	0.015	0.629	0.365
	333.15	0.754	0.004	0.241	0.001	0.752	0.240
	333.15	0.812	0.004	0.184	0.002	0.812	0.180
	333.15	0.281	0.004	0.710	0.004	0.282	0.715
liquid phase	T/K	x_1	δx_1	x_2	δx_2	x_1 (HYSYS)	x_2 (HYSYS)
	333.15	0.363	0.005	0.035	0.001	0.344	0.036
	333.15	0.424	0.007	0.030	0.000	0.407	0.030
	333.15	0.497	0.011	0.022	0.001	0.490	0.022
	333.15	0.553	0.003	0.018	0.001	0.534	0.018
	333.15	0.202	0.007	0.049	0.001	0.190	0.049

slightly polar solvents. The polarity of nonanal is significantly higher than 1-octene.

Table 13 summarizes the enhancement factor (EF) for CO solubility in CO_2-expanded nonanal relative to that in neat nonanal at identical temperature and gas phase CO fugacities. Once again, EF values are greater than 1 and increase with increasing CO_2 content in the liquid phase at constant temperature and total pressure, as shown by a comparison with Table 12. A comparison of Tables 9 and 13 shows that the enhancement of CO solubility is greater in nonanal than in 1-octene.

CO_2 + H_2 + 1-Octene. Figure 14 shows the VLE of H_2 + 1-octene mixtures were measured at (313.15 and 333.15) K and at pressures between (1 and 8) MPa. The data are summarized in Table 14. The experimental errors are within the size range of the data points. In general, while the H_2 solubility increased with total pressure, the temperature had a relatively weak effect on H_2 solubility.

The VLE data of CO_2 + H_2 + 1-octene at 8 MPa and (313.15 and 333.15) K are shown in Table 15, as are the simulated data.

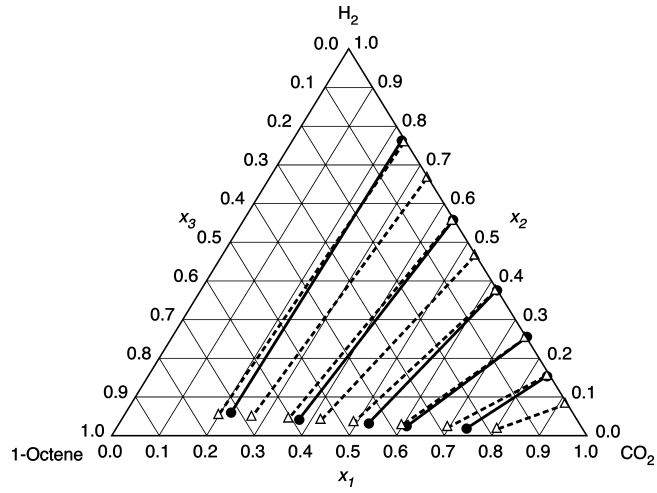

Figure 15. Vapor−liquid equilibrium of ternary mixtures CO_2 (1) + H_2 (2) + 1-octene (3) at T = 313.15 K and p = 8 MPa. Mole fractions x_i. —●—, Experimental data; and --Δ--, HYSYS simulation data.

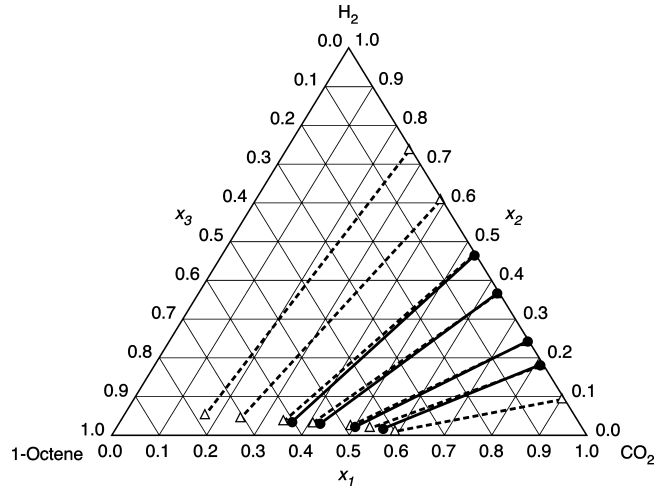

Figure 16. Vapor−liquid equilibrium of ternary mixtures CO_2 (1) + H_2 (2) + 1-octene (3) at T = 333.15 K and p = 8 MPa. Mole fractions x_i. —●—, Experimental data; and --Δ--, HYSYS simulation data.

Table 16. Enhancement Factor EF of H_2 Solubility in Pure Octene (1) and CXL−Octene (2) as a Function of H_2 Fugacity f_{H2} at T = (313.15 and 333.15) K

T/K	f_{H2}/MPa	x_1	x_2	EF
313.15	1.26	0.010	0.017	1.65
313.15	2.02	0.017	0.023	1.39
313.15	2.99	0.025	0.030	1.22
313.15	4.46	0.037	0.040	1.09
313.15	6.10	0.049	0.051	1.04
333.15	1.47	0.012	0.018	1.44
333.15	1.92	0.016	0.022	1.34
333.15	2.92	0.025	0.030	1.21
333.15	3.71	0.032	0.035	1.10
333.15	5.68	0.048	0.049	1.02

The experimental and simulated VLE data for this system are compared in Figures 15 and 16. Table 8 summarizes the fit between experimental and simulated VLE data using AARD. In general, the experimental and simulated results show reasonably good agreement considering that only binary interaction parameters were used.

Table 16 summarizes the EF for H_2 solubility in CO_2-expanded 1-octene relative to that in neat 1-octene at identical temperature and gas phase H_2 fugacities. As with CO solubility, EF values exceeding 1 are obtained for all conditions studied, and EF values increase with increasing CO_2 content in the liquid

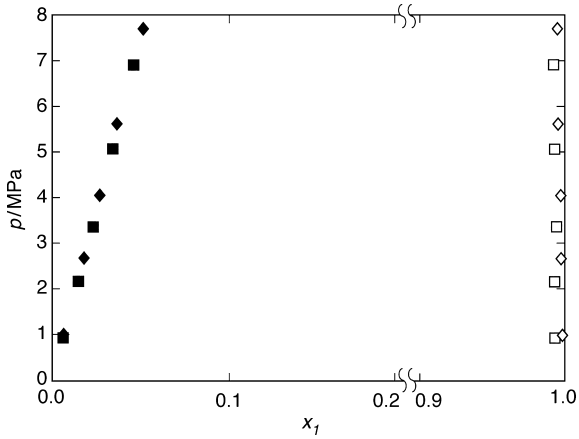

Figure 17. Vapor−liquid equilibrium of binary mixtures H_2 (1) + nonanal (2) at pressure p = (0 to 8) MPa. Mole fractions x_1. ◆, 313.15 K, liquid phase; ◇, 313.15 K, vapor phase; ■, 333.15 K, liquid phase; and □, 333.15 K, vapor phase.

Table 17. Vapor Phase Mole Fraction y_1, Standard Deviation δy_1, Liquid Phase Mole Fraction x_1, and Standard Deviation δx_1 for H_2 (1) + Nonanal (2) Binary Mixtures at T = (313.15 and 333.15) K and Total p from (0 to 8) MPa

T/K	p/MPa	x_1	δx_1	y_1	δy_1
313.15	1.01	0.006	0.001	0.999	0.001
313.15	2.69	0.018	0.001	0.997	0.002
313.15	4.06	0.027	0.001	0.998	0.002
313.15	5.63	0.037	0.001	0.995	0.001
313.15	7.71	0.052	0.002	0.995	0.001
333.15	0.94	0.006	0.001	0.993	0.001
333.15	2.18	0.015	0.001	0.993	0.001
333.15	3.37	0.023	0.001	0.994	0.001
333.15	5.07	0.034	0.001	0.993	0.001
333.15	6.91	0.046	0.001	0.992	0.001

phase at constant temperature and total pressure, as shown by a comparison with Table 15. The dissolved CO_2 serves to increase the free volume in the CXL phase, enhancing the H_2 solubility.

CO_2 + H_2 + Nonanal. Figure 17 shows the VLE of H_2 + nonanal mixtures were measured at (313.15 and 333.15) K and at pressures between (1 and 8) MPa. The data are summarized in Table 17. In general, while the H_2 solubility increased with total pressure, the temperature had a relatively weak effect on H_2 solubility.

The VLE data of H_2 + CO_2 + nonanal at (313.15 and 333.15) K and at pressure 8 MPa are shown in Table 18, in addition to the simulated data. The experimental and simulated VLE data for this system are compared in Figures 18 and 19. Table 8 summarizes the fit between experimental and simulated VLE data using AARD. Once again, the experimental and simulated results show reasonably good agreement considering that only binary interaction parameters were used. As was the case with CO, the simulated results for nonanal-based systems are not as good as for 1-octene systems.

Table 19 summarizes the EF for H_2 solubility in CO_2-expanded nonanal relative to that in neat nonanal at identical temperature and gas phase H_2 fugacities. As before, EF values exceeding 1 are obtained for all conditions studied, and EF values increase with increasing CO_2 content in the liquid phase at constant temperature and total pressure, as shown by a comparison with Table 18. A comparison of Tables 16 and 19 shows that the enhancement of H_2 solubility is greater in nonanal than in 1-octene.

Table 18. Vapor Phase Mole Fractions y_1, y_2, Standard Deviations δy_1, δy_2, Liquid Phase Mole Fractions x_1, x_2, and Standard Deviations δx_1, δx_2 for CO_2 (1) + H_2 (2) + Nonanal (3) Ternary Mixtures at T = (313.15 and 333.15) K and Total p = 8 MPa

vapor phase	T/K	y_1	δy_1	y_2	δy_2	y_1 (HYSYS)	y_2 (HYSYS)
	313.15	0.153	0.002	0.837	0.002	0.153	0.847
	313.15	0.431	0.002	0.562	0.005	0.432	0.568
	313.15	0.556	0.004	0.438	0.003	0.557	0.443
	313.15	0.682	0.004	0.312	0.004	0.684	0.316
	313.15	0.811	0.004	0.183	0.004	0.813	0.186
liquid phase	T/K	x_1	δx_1	x_2	δx_2	x_1 (HYSYS)	x_2 (HYSYS)
	313.15	0.163	0.008	0.046	0.003	0.150	0.045
	313.15	0.419	0.010	0.035	0.002	0.383	0.033
	313.15	0.510	0.002	0.029	0.001	0.479	0.028
	313.15	0.592	0.009	0.024	0.001	0.577	0.022
	313.15	0.715	0.010	0.018	0.002	0.686	0.015
vapor phase	T/K	y_1	δy_1	y_2	δy_2	y_1 (HYSYS)	y_2 (HYSYS)
	333.15	0.220	0.005	0.775	0.004	0.220	0.780
	333.15	0.379	0.002	0.615	0.015	0.380	0.620
	333.15	0.551	0.004	0.442	0.001	0.553	0.447
	333.15	0.732	0.004	0.262	0.002	0.735	0.265
	333.15	0.863	0.004	0.130	0.004	0.868	0.132
liquid phase	T/K	x_1	δx_1	x_2	δx_2	x_1 (HYSYS)	x_2 (HYSYS)
	333.15	0.190	0.005	0.044	0.001	0.171	0.042
	333.15	0.297	0.007	0.037	0.000	0.280	0.035
	333.15	0.439	0.011	0.028	0.001	0.412	0.026
	333.15	0.553	0.003	0.020	0.001	0.508	0.018
	333.15	0.617	0.007	0.013	0.001	0.591	0.012

Conclusions

The vapor−liquid equilibria of the following binary and ternary systems were measured in a variable volume view cell at temperatures ranging from (313.15 to 353.15) K and pressures up to 9 MPa: CO + 1-octene, CO_2 + 1-octene, CO + 1-octene + CO_2, CO + nonanal, CO_2 + nonanal, CO + nonanal + CO_2, H_2 + 1-octene, H_2 + 1-octene + CO_2, H_2 + nonanal, and H_2 + nonanal + CO_2. The vapor and liquid phases at equilibrium were sampled at constant pressure and analyzed using a gas chromatograph.

The solubilities of CO, H_2, and CO_2 in the solvents were consistent with literature values. The increase of temperature

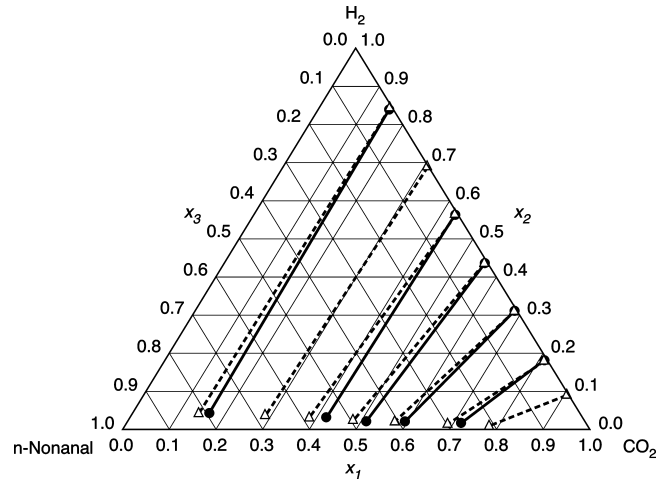

Figure 18. Vapor−liquid equilibrium of ternary mixtures CO_2 (1) + H_2 (2) + nonanal (3) at T = 313.15 K and p = 8 MPa. Mole fractions x_i. —●—, Experimental data; and --Δ--, HYSYS simulation data.

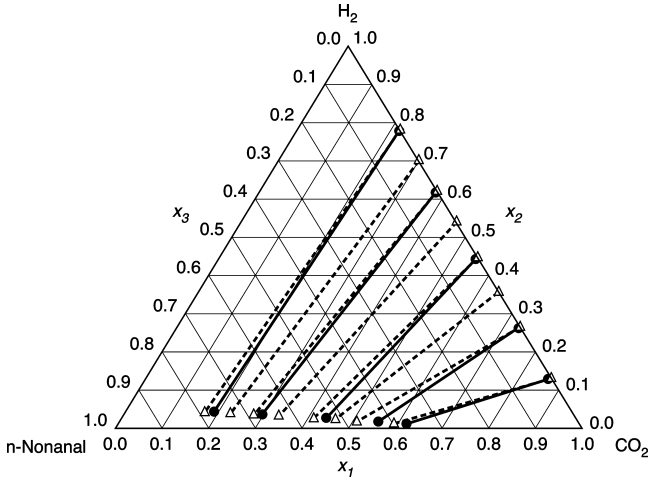

Figure 19. Vapor−liquid equilibrium of ternary mixtures CO_2 (1) + H_2 (2) + nonanal (3) at $T = 333.15$ K and $p = 8$ MPa. Mole fractions x_i. —●—, Experimental data; and --Δ--, HYSYS simulation data.

Table 19. Enhancement Factor EF of H_2 Solubility in Pure Nonanal (1) and CXL−Nonanal (2) as a Function of H_2 Fugacity f_{H2} at T = (313.15 and 333.15) K

T/K	f_{H2}/MPa	x_1	x_2	EF
313.15	1.50	0.010	0.018	1.82
313.15	2.56	0.017	0.024	1.40
313.15	3.59	0.023	0.029	1.24
313.15	4.61	0.030	0.035	1.15
313.15	6.86	0.044	0.046	1.04
333.15	1.07	0.007	0.013	1.76
333.15	2.15	0.014	0.020	1.36
333.15	3.62	0.024	0.028	1.17
333.15	5.04	0.033	0.037	1.10
333.15	6.36	0.042	0.044	1.05

almost had no effect on the solubility of CO or H_2 in the solvents. The increase of temperature reduced the solubility of CO_2 in the solvents.

The presence of CO_2 enhanced the solubilities of both CO and H_2 in the liquid phase. The enhancement factor (EF) was up to 1.54 for carbon monoxide and 1.82 for hydrogen. EF values greater than 1 were obtained for all conditions studied. At constant temperature and total pressure, EF increased with the increase of CO_2 in the liquid phase. The enhancements of syngas solubility are higher in product mixtures (CXL−nonanal) than in reactant mixtures (CXL−octene).

The Peng−Robinson equation of state (PR EoS) with van der Waals mixing rules and binary interaction parameters modeled the VLE data adequately, with much better fits for the 1-octene systems compared to the more polar nonanal systems.

Acknowledgment

It is a distinct privilege to be invited to contribute to this festschrift honoring Professor Gerhard M. Schneider from whose outstanding research contributions we have learned a great deal about high pressure phase equilibrium thermodynamics.

Literature Cited

(1) Jessop, P. G.; Subramaniam, B. Gas-Expanded Liquids. *Chem. Rev.* **2007**, *107*, 2666–2694.
(2) Jin, H.; Subramaniam, B.; Ghosh, A.; Tunge, J. Intensification of catalytic olefin hydroformylation in CO_2-expanded media. *AIChE J.* **2006**, *52*, 2575–2581.
(3) Katayama, T.; Ohgaki, K.; Maekawa, G.; Goto, M.; Nagano, T. Isothermal vapor-liquid equilibriums of acetone-carbon dioxide and methanol-carbon dioxide systems at high pressures. *J. Chem. Eng. Jpn.* **1975**, *8*, 89–92.
(4) Brunner, E. Solubility of hydrogen in 10 organic solvents at 298.15, 323.15, and 373.15 K. *J. Chem. Eng. Data* **1985**, *30*, 269–273.
(5) Purwanto, P.; Deshpande, R. M.; Chaudhari, R. V.; Delmas, H. Solubility of Hydrogen, Carbon Monoxide, and 1-Octene in Various Solvents and Solvent Mixtures. *J. Chem. Eng. Data* **1996**, *41*, 1414–1417.
(6) Jáuregui-Haza, U. J.; Pardillo-Fontdevila, E. J.; Wilhelm, A. M.; Delmas, H. Solubility of hidrogen and carbon monoxide in water and some organic solvents. *Lat. Am. Appl. Res.* **2004**, *34*, 71–74.
(7) Kaminishi, G.; Toriumi, T. Vapor-liquid equilibria in the systems: carbon dioxide-carbon monoxide, carbon dioxide-carbon monoxide-hydrogen, carbon dioxide-methane. *Rev. Phys. Chem. Jpn.* **1968**, *38*, 79–84.
(8) Christiansen, L. J.; Fredenslund, A.; Gardner, N. Gas-liquid equilibriums carbon dioxide-carbon monoxide and carbon dioxide-methane-carbon monoxide systems. *Adv. Cryog. Eng.* **1974**, *19*, 309–319.
(9) Christov, M.; Dohrn, R. High-pressure fluid phase equilibria: Experimental methods and systems investigated (1994−1999). *Fluid Phase Equilib.* **2002**, *202*, 153–218.
(10) Schneider, G. M. High-pressure investigations of fluid mixtures-review and recent results. *J. Supercrit. Fluids* **1998**, *13*, 5–14.
(11) Bezanehtak, K.; Dehghani, F.; Foster, N. R. Vapor-Liquid Equilibrium for the Carbon Dioxide + Hydrogen + Methanol Ternary System. *J. Chem. Eng. Data* **2004**, *49*, 430–434.
(12) Xie, X.; Brown, J. S.; Bush, D.; Eckert, C. A. Bubble and Dew Point Measurements of the Ternary System Carbon Dioxide + Methanol + Hydrogen at 313.2 K. *J. Chem. Eng. Data* **2005**, *50*, 780–783.
(13) Yin, J.-Z.; Tan, C.-S. Solubility of hydrogen in toluene for the ternary system H_2 + CO_2 + toluene from 305 to 343 K and 1.2 to 10.5 MPa. *Fluid Phase Equilib.* **2006**, *242*, 111–117.
(14) Lopez-Castillo, Z. K.; Aki, S. N. V. K.; Stadtherr, M. A.; Brennecke, J. F. Enhanced Solubility of Oxygen and Carbon Monoxide in CO_2-Expanded Liquids. *Ind. Eng. Chem. Res.* **2006**, *45*, 5351–5360.
(15) Zevnik, L.; Levec, J. Hydrogen solubility in CO_2-expanded 2-propanol and in propane-expanded 2-propanol determined by an acoustic sensor. *J. Supercrit. Fluids* **2007**, *41*, 335–342.
(16) Lopez-Castillo, Z. K.; Aki, S. N. V. K.; Stadtherr, M. A.; Brennecke, J. F. Enhanced Solubility of Hydrogen in CO_2-Expanded Liquids. *Ind. Eng. Chem. Res.* **2008**, *47*, 570–576.
(17) Houndonougbo, Y.; Jin, H.; Rajagopalan, B.; Kuczera, K.; Subramaniam, B.; Laird, B. B. Phase Equilibria in Carbon Dioxide Expanded Solvents: Experiment and Molecular Simulations. *J. Phys. Chem. B* **2006**, *110*, 13195–13202.
(18) Houndonougbo, Y.; Kuczera, K.; Subramaniam, B.; Laird, B. B. Prediction of the Phase Equilibria and Transport Properties in Carbon-Dioxide Expanded Solvents by Molecular Simulation. *Mol. Simul.* **2007**, *33*, 861–869.
(19) Guha, D.; Jin, H.; Dudukovic, M. P.; Ramachandran, P. A.; Subramaniam, B. Mass Transfer Effects during Homogeneous 1-Octene Hydroformylation in CO2-expanded Solvent: Modeling and Experiments. *Chem. Eng. Sci.* **2007**, *62*, 4967–4975.
(20) Clevett, K. J. *Process analyzer technology*; Wiley: New York, 1986.
(21) Day, C. Y. Phase Equilibrium of Ethanol + CO_2 and Acetone + CO_2 at Elevated Pressures. *J. Chem. Eng. Data* **1996**, *41*, 839–843.
(22) Jin, H. *Exploiting carbon dioxide-expanded liquids as reaction media for catalytic hydroformylation of higher olefins*; University of Kansas: Lawrence, 2006.
(23) Bonate, P. L. Concepts in calibration theory. Part I: regression. *LC-GC* **1992**, *10*, 310–314.
(24) Bonate, P. L. Concepts in calibration theory. Part IV. Prediction and confidence intervals. *LC-GC* **1992**, *10*, 531–532.
(25) Bonate, P. L. Concepts in calibration theory. Part II: regression through the origin-when should it be used. *LC-GC* **1992**, *10*, 378–379.
(26) Bonate, P. L. Concepts in calibration theory, part III: weighted least-squares regression. *LC-GC* **1992**, *10*, 448–450.

Received for review February 2, 2009. Accepted March 27, 2009. This research was partly supported by the National Science Foundation Engineering Research Center Grant (EEC-0310689).

JE900148E